

Linking Large-Eddy Simulations to local cloud observations

Vera Schemann¹, Kerstin Ebell¹, Bernhard Pospichal¹, Roel Neggers¹,
Christopher Moseley, and Bjorn Stevens³

¹Institute of Geophysics and Meteorology, University of Cologne, Cologne, Germany

²Department of Atmospheric Sciences, National Taiwan University, Taipei 10617, Taiwan

³Max Planck Institute for Meteorology, Hamburg, Germany

Key Points:

- How can we bridge the gap between ground-based observations of the atmospheric column and weather/climate models?
- For comparison with these observations (esp. measurements of the vertical column) it is important to take external variability (e.g. large scale forcing and surface) into account.
- ICON-LEM offers new possibilities to simulate small scales while considering external variability.

Corresponding author: Vera Schemann, vera.schemann@uni-koeln.de

16 **Abstract**

17 Linking large-eddy simulations to local observations of clouds enables us to investigate
 18 clouds and microphysical processes and to improve our understanding as well as the re-
 19 spective representation in coarser models. Insights gained with large-eddy simulations
 20 can be applied within the development and evaluation of parameterizations for larger
 21 scale models, to bridge the gap between those models and the detailed local observations.
 22 In this study, various approaches for large-eddy simulations around local observations
 23 are explored and investigated with respect to remote sensing observations of clouds and
 24 their representation. By adding more 'realism' to the simulations and defining a well con-
 25 strained setup, the representation of the daily variability at a mid-latitude site could be
 26 improved and shows promising results for continued research in the future. Especially
 27 the shown potential to investigate representativeness of column measurements will pro-
 28 vide new insights into the analysis and construction of observational experiments.

29 **Plain Language Summary**

30 Clouds are still a cause for uncertainty in our understanding of climate and climate
 31 feedbacks. Due to the large range of involved scales – from small droplets up to storm
 32 systems – their representation in weather and climate models is an ongoing challenge.
 33 While new and sophisticated measurements of the atmospheric column could provide new
 34 insights into important processes, their linking to models is not trivial and is ongoing
 35 research. In this study, we are presenting and exploring different approaches to combine
 36 local observations of clouds with state-of-the-art high-resolution simulations. And we are
 37 presenting a setup, which shows a promising representation of the observed clouds and
 38 is constrained enough to be applicable for long-term statistics – one of the key require-
 39 ments for improvements and evaluation clouds in of weather and climate models.

40 **1 Introduction**

41 Clouds and cloud feedback mechanisms have, for quite some time, contributed sub-
 42 stantial uncertainty to estimates of how the climate system responds to radiative forc-
 43 ing (Cess et al., 1990; Bony et al., 2006; Boucher et al., 2013; Stevens et al., 2016). Even
 44 as a new generation of climate models, with kilometer scale horizontal meshes, are show-
 45 ing great promise for better representing precipitation processes (Satoh et al., 2019; Stevens
 46 et al., 2019), clouds remain challenging to represent, with expected, but largely unquan-
 47 tified sensitivity to cloud microphysical processes (Stevens et al., 2020). An ability to
 48 accurately represent clouds in meteorological models is important for all types of weather
 49 forecasts, but also new application sectors such as renewable energy. For these reasons
 50 there has been a tremendous effort over the past decades to improve observations, sim-
 51 ulations, and models of cloud processes, as well as interest in new methods for harmo-
 52 nizing these methodologies (Schneider et al., 2017).

53 In a new twist on an old approach, Schneider et al. (2017) propose to spawn mul-
 54 titudes of idealized large-eddy simulations for the large-scale conditions associated with
 55 important cloud regimes. The simulations would then be constrained by satellite data,
 56 and their dynamics would be learned by machines. Advances in computing, and in ma-
 57 chine learning, would thus allow the replication of the GCSS (GEWEX (Global Energy
 58 and Water Experiment) Cloud Systems Studies) approach outlined by Browning et al.
 59 (1993) on a massive scale. The GCSS approach, like its more modern incarnation, adopts
 60 the scale-separation hypothesis inherent to the parameterization problem; whereby it is
 61 assumed that small scale processes respond to much larger-scale forcing, to set the prop-
 62 erties of clouds and precipitation. This assumption gives relevance to the study of the
 63 dynamics of very high-resolution simulations over very small domains for large-scale con-
 64 ditions that are prescribed and stationary. Essentially it allows for the study of quite ide-
 65 alized problems, whereby heterogeneity of any kind in the forcing is neglected. The sim-

66 ulation of stratocumulus idealized from observations taken during the First ISCCP (In-
67 ternational Satellite Cloud Climatology Project) Regional Experiment (FIRE) is an early
68 example of this approach (Moeng et al., 1996). But over the years there have been a great
69 many studies of this kind and the approach, can under some conditions yield quite sat-
70 isfactory results, and remains quite popular (Holloway et al., 2014), and – forshadow-
71 ing its almost industrial application as suggested by Schneider et al. (2017) – has begun
72 to be applied also to routine observations from local sites (Neggers et al., 2012; Schalk-
73 wijk et al., 2015).

74 Parallel to these developments some groups have been experimenting with approaches
75 that relax the parameterization assumption, by embedding smaller domain very high-
76 resolution simulations in a more dynamic large-scale environment. Notably Chow et al.
77 (2006) embedded LES in a mesoscale model to study boundary layer processes over com-
78 plex terrain, an approach developed simultaneously and applied to idealized problems
79 by Moeng et al. (2007). In doing so, Chow et al. (2006) noted the importance of an ac-
80 curate representation of surface forcing, but also sensitivities to how the nested simu-
81 lations were set up, an issue also investigated by Moeng et al. (2007). In a later, related
82 study, adopting a similar approach of nesting a Large-Eddy Simulation within larger-
83 scale mesoscale model, Talbot et al. (2012) also highlight the importance of the mesoscale
84 meteorological forcing for the LES. These approaches make it possible to use observa-
85 tions from regions, or for time-periods, where there is not a strong separation between
86 the large and small scales. As computational capacity has increased it has also become
87 possible to simply do away with the nesting and begin performing large-eddy simulations
88 over very large domains, thereby coupling the mesoscale with the turbulence scale more
89 organically, and allowing the representation of more realistic situations (Heinze, Dipankar,
90 et al., 2017; Stevens et al., 2020).

91 In this study, we systematically explore the trade-offs associated with some of the
92 different approaches outlined above. For instance, the benefits of a large-domain which
93 allows a realistic coupling between turbulent and mesoscale motions, versus a local do-
94 main which might allow a tighter prescription of the large-scale flow and a higher res-
95 olution representation of turbulent processes. In the latter case one can further ask how
96 much additional information is imprinted by heterogeneity in the lower boundary con-
97 dition, or through the open boundary conditions. To perform the study we take advan-
98 tage of and expand upon the capabilities of the large-eddy simulation model configura-
99 tion of ICON (ICON-LEM; Dipankar et al., 2015). ICON can be run with open lateral
100 boundary conditions and a heterogeneous and complex surface over very large domains
101 (Heinze, Dipankar, et al., 2017) as well as in semi-idealized mode (Heinze, Moseley, et
102 al., 2017), or with the small and computationally more efficient setup as used in Marke
103 et al. (2018) and Schemann and Ebell (2020). In this study, with applications such as
104 the LES Symbiotic simulation and observation workflow (LASSO; W. Gustafson et al.,
105 2019) in mind, we also include in our comparison suite simulations with the Dutch At-
106 mospheric Large-Eddy Model (DALES; Heus et al., 2010).

107 The focus of our study will be on the representation of clouds through the vary-
108 ing approaches to perform LES around local observations. As a reference site for com-
109 parison, we choose the Jülich Observatory for Cloud Evolution (JOYCE, Löhnert et al.
110 (2015)), which provides several remote sensing observations and is surrounded by an area
111 of modest heterogeneity. But in general, the setups should be applicable for different lo-
112 cations and conditions.

113 The manuscript is organized as follow: In Sec. 2 the different model setups as well
114 as the observational basis of evaluation is introduced. This will be followed by a basic
115 comparison (Sec. 3) and a discussion of the resolution dependency (Sec. 4) as well as the
116 dependency on different forcing data. Further details, such as the role of the modest to-
117 pography in the study area, are explored through the analysis of a specific case study

118 in Sec. 5. We conclude, as is customary with a brief summary and a restatement of our
 119 major findings.

120 2 Model setup and Data

121 Different models and model configurations (see Tab. 1) are applied to study the
 122 weaknesses and strengths in their ability to capture different synoptic conditions, on the
 123 one hand, and the details provided by measurements, on the other hand. Simulations
 124 are compared to observations from the measurement site JOYCE (Löhnert et al., 2015).
 125 In this section, the different model setups as well as the observational site and its data
 126 are introduced. References are provided for information already in the published liter-
 127 ature.

Setup	Top	Domain size	Horz. Mesh	Boundary conditions
ICON-DE	21 km	1000 km	156 m	O/Het (C)
“	“	“	312 m	“
“	“	“	624 m	“
ICON-LOC	”	20 km	78 m	O/Het (C,I)
“	”	30 km	156 m	“
“	”	60 km	312 m	“
“	”	110 km	624 m	“
ICON-SI	13 km	7 km	50 m	P/Hom (C)
DALES-SI	5 km	6.4 km	50 m	P/Hom (I)

Table 1. Overview of the applied model setups summarizing the height of the model top, the domain size (linear dimension), horizontal mesh size (linear dimension), and boundary conditions. Boundary conditions are either open and heterogeneous (O/Het) and thus including different surface types as well as topography, or Periodic (lateral) and homogeneous (surface) as designated by P/Hom. Boundary conditions are provided by either COSMO-DE (C) or the ECMWF-IFS (I).

128 Often the word “resolution” is used as short hand for the grid spacing. As many
 129 studies have shown, they are not the same thing, but the former generally scales with
 130 the latter, and we use the terms synonymous. In addition, at least for the ICON model
 131 there is also ambiguity in what is meant by grid spacing. Values given in Tab. 1, mea-
 132 sure the edge length of a grid-cell, which – due to the triangular grid – has to be scaled
 133 by a factor of $2/3$ to provide an area-based resolution. Hence an edge length of 78 m cor-
 134 responds to a 50 m area-based resolution, however each cell has less information than in
 135 a rectangular grid, i.e., because the velocities are defined on cell faces, triangles come with
 136 three velocities instead of four. This is expected to impact (reduce) the resolution for
 137 a given grid spacing as compared to a quadrilateral discretization.

138 2.1 Analyzed time period

139 To capture different synoptic situations and investigate the overall performance as
 140 well as looking into specific case studies, our study focuses on 9 d of the Observational
 141 Prototype Experiment (HOPE; Macke et al., 2017). HOPE comprised a 2 month field
 142 study in the vicinity of Jülich, Germany, during April and May 2013. The time period

143 24 April 2013 to 2 May 2013 was chosen to allow the use of previously performed sim-
 144 ulations with the very large domain (ICON-DE). Within this period, two (relatively) clear-
 145 sky days were followed by a passage of a frontal system (26 and 27 April). The rest of
 146 the period consisted of more mixed conditions with the exception of two days with shal-
 147 low cumulus clouds (1 and 2 May). Hence, we can investigate the performance of the dif-
 148 ferent models and model configurations for different atmospheric situations.

149 2.2 Realistic setup (ICON-LEM)

150 What we call the 'realistic' set-up of the ICON-LEM (Large-Eddy Model) is one
 151 where the simulations are subject to lateral boundary and surface conditions that attempt
 152 to mimic reality as closely as possible. For the surface conditions this includes both the
 153 specification of the topography and the land-surface properties. As a default these sim-
 154 ulations are initialized and forced every hour with output from the COSMO-DE, the op-
 155 erational numerical weather prediction model of the German Meteorological Service (Deutscher
 156 Wetterdienst, DWD) with a grid spacing of 2.8 km (e.g. Baldauf et al., 2011). As described
 157 below, both large and small domain simulations are performed using the realistic set up.
 158 The small domain simulations (ICON-LOC) are performed twice, once with the COSMO-
 159 DE forcing and once with forcing data from the Integrated Forecasting System (IFS) of
 160 the European Centre for Medium-range Weather forecasts (ECMWF). This allows us
 161 to assess the sensitivity to uncertainty in the boundary and initial data.

162 The large-domain simulations (ICON-DE) cover the whole of Germany (Fig. 1, left)
 163 which allows mesoscale processes to develop and interact freely with smaller scale, tur-
 164 bulent, features as are the normal focus of LES. The simulations incorporate two nests.
 165 Each nest refines the grid spacing by a factor of two, and slightly reduces the size of the
 166 domain to smooth the change in grid-spacing at the lateral boundaries. Compared to
 167 the domain as a whole these transition regions are very small, and because the nesting
 168 is one way, this effectively provides three simulations with progressively refined meshes
 169 (from 624 m to 156 m) over all of Germany. The ICON-DE simulations have been per-
 170 formed within the HD(CP)² project (Heinze, Dipankar, et al., 2017; Stevens et al., 2020)
 171 and are used as a reference. They are very computationally expensive, and thus have been
 172 performed only for selected days (24-26 April 2013, 2 May 2013).

173 The ICON-LOC simulations are a smaller version of the ICON-DE simulations. They
 174 start with a domain size of 110 km and a 624 m grid mesh. They are nested three times
 175 with the smallest domain having a size of ca. 20 km and 78 m resolution (Fig. 1, mid-
 176 dle). Like the ICON-DE simulations the one-way nesting effectively results in four sim-
 177 ulations as described in Table 1. To reduce the computation expense and allow yet finer
 178 scale simulations, the domain size of each finer mesh is reduced more than is done for
 179 the ICON-DE simulations, combined with the smaller sizes of the domains to begin with
 180 this results in roughly a factor of two reduction in the domain size with each factor of
 181 two reduction in mesh size. An obvious advantage of the small domains is the limited
 182 computational demand, which allows the whole analysis period to be simulated. ICON's
 183 unstructured mesh and the use of open boundary conditions made it possible to define
 184 a roughly circular domain, centered on the JOYCE observational site. By choosing a cir-
 185 cular domain the quality of the simulation should not be effected by the direction of the
 186 flow. Experiments were performed with domains of different sizes, but systematic dif-
 187 ferences were difficult to identify and this aspect of the set-up was not further explored.

188 All of the ICON setups share the same set of parameterizations including a Smagorin-
 189 sky turbulence scheme (see Dipankar et al. (2015) for more details). For the cloud mi-
 190 crophysics parameterization, the two-moment scheme by Seifert and Beheng (2006) is
 191 used, which is based on six hydrometeor classes (liquid, ice, rain, snow, graupel, hail).
 192 The model nesting is for both setups one-way. This means that information is only pro-

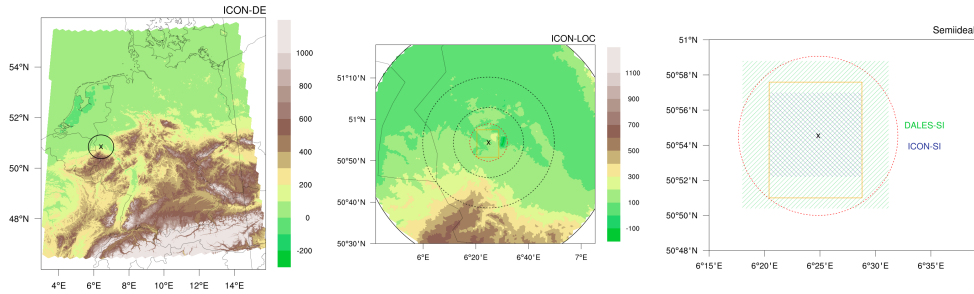


Figure 1. Model domains of the different setups. Left: ICON-DE. The circle indicates the domain of the ICON-LOC; middle: ICON-LOC with the 4 nested domains; right: sketch for domain size of DALES-SI (green shading), ICON-SI (blue shading) and ICON-LOC for smallest domain. The x indicates the location of JOYCE, and the orange rectangle encloses the subdomain used in the analysis. For ICON-DE and ICON-LOC, the colors show the topography (in m).

193 vided from the coarser to the finer resolutions. For both realistic configurations (ICON-
194 DE and ICON-LOC) 150 levels are used, reaching up to 21 km.

195 For the realistic simulations, we have different output possibilities. For most of our
196 analysis we will use the “meteogram” output. This consists of quantities taken from the
197 model column closest to the location of the observational site. In case of the ICON-LOC
198 setup, this is the center of the domain. As it is only the output of one column, the out-
199 put frequency is rather high with every 9 seconds. This output is designed to mimic how
200 we observe the atmosphere with automated measurements, but it provides no (horizontal-
201 tal) spatial information, which is the main drawback of this type of output.

202 For comparison and to investigate the question of how valid the point-to-point eval-
203 uation is and how we can use models to put column observations into a 3 dimensional
204 context, we also use 2D information of vertically integrated quantities. The output fre-
205 quency of the 2D data for the ICON-LOC is every 10 minutes.

206 2.3 Semi-idealized setup (DALES and ICON-LEM)

207 What we call the semi-idealized simulations follow the more traditional way of con-
208 figuring and performing large-eddy simulation. These simulations are idealized in that
209 they adopt a simplified surface forcing (i.e. homogeneous land surface types) and peri-
210 odic horizontal boundary conditions. In addition, the large scale forcing (both horizon-
211 tal advection and subsidence) is applied in a horizontally homogeneous way, meaning that
212 all columns experience the same associated tendencies. We use the term “semi-idealized”
213 in this study, to point out, that we still use time-varying large-scale forcing in order to
214 introduce changes in the synoptic situation – the weather – to the LES instead of stick-
215 ing to one special case (Neggers et al., 2012). The ICON-LEM model also offers the pos-
216 sibility to be run in a more fully idealized mode (Heinze, Moseley, et al., 2017). How-
217 ever this set up is less well tested. For this reason we decided to also include results from
218 a more well established model, DALES (Heus et al., 2010) . The DALES model has al-
219 ready been used for semi-idealized simulations (Neggers et al., 2012) over a wide vari-
220 ety of conditions (van Laar et al., 2019; Neggers et al., 2019; Reilly et al., 2020). The
221 model version that has been used for this study (DALES-SI) only takes warm microphysics
222 (without ice) into account.

Whereas the ICON-LEM semi-idealized version (ICON-SI) (Heinze, Moseley, et al., 2017)) is forced with COSMO-DE data, the DALES-SI is forced with IFS data. The exact construction of the IFS forcing is described by van Laar et al. (2019). For semi-idealized simulations, different forcing datasets can result in different atmospheric conditions. For our study, this is an advantage as we would like to span a rather wide range of possible outcomes from semi-idealized models to investigate how close they can come to observations and how they compare to the more realistic setup. A sketch of the model domain of DALES-SI and ICON-SI as well as the domain size of the innermost domain of ICON-LOC can be seen in Fig. 1 (right).

For the analysis of the semi-idealized simulations we mostly focus on domain mean output. The DALES model additionally offers the possibility to have a vertical cross-section output with a frequency of 30 seconds, these are used for the hydrometeor classifications. For the ICON-LEM, we added 2D output for integrated values every 10 minutes similar to what is done for the realistic setup.

2.4 Observations (JOYCE)

The observations used in this study were performed at JOYCE, the Jülich Observatory for Cloud Evolution (Löhnert et al., 2015). JOYCE was founded in 2008 and became a comprehensive site for ground-based observations of the atmosphere with the main focus on profiling clouds, precipitation, wind, and the thermodynamic state of the atmospheric column using different remote sensing methods. The observations are performed by several cloud and precipitation radars, a microwave radiometer, Doppler lidar, ceilometer, and various other instruments. All these measurements are performed continuously with a temporal resolution of less than a minute. In 2013, JOYCE was part of the HOPE campaign (Macke et al., 2017) where additional ground-based remote sensing instruments were installed in the vicinity of JOYCE to observe local variability. Observational data from HOPE will be used in this study.

Since 2011, JOYCE is part of the European network Cloudnet (Illingworth et al., 2007) within the European Research Infrastructure for the observation of Aerosol, Clouds and Trace Gases (ACTRIS). The Cloudnet network consists of currently 15 stations around Europe which operate the combination of cloud radar, microwave radiometer and ceilometer. From these observations, Cloudnet provides many cloud properties, such as classification (phase, precipitation), extent and liquid water/ice water content on a constant temporal (30 s) and vertical grid (30 m).

3 Capturing the weather

To enable the comparison of simulations around heavily instrumented observational sites, it is important to capture the general weather or synoptic conditions. These large-scale features should be provided by the forcing model, while the high-resolution model should resolve and focus on the small-scale features like turbulence and clouds within the given weather regime. To evaluate the representation of the general weather, we compare the integrated water vapor (IWV), which is a good measure for the synoptic structure. As the evolution of the IWV will be dominated by the large scale forcing models it proves sufficient to compare this quantity from the ICON-LOC 78 m and the ICON-SI, as two examples covering the range of model configurations. Given that we are first interested in whether the general weather situation is well captured, we calculated a 30-minute running mean of the IWV for the period 29 April to 2 May 2013. Figure 2 (top) shows a good agreement of the simulated IWV and the observed one. Even though the information is given at the boundaries in the ICON-LOC setup, while the output is taken in the center, it covers nicely the increase and decrease of the IWV over the 9 d. Whereas the IWV is dominated by the large scales, the cloud liquid water path (LWP) provides an estimate of the model's ability to represent the small scales through the the liquid

cloud occurrence. With respect to the liquid cloud occurrence, the simulations differ more markedly. ICON-LOC shows a reasonable agreement with the observations (Fig. 2 bottom) while ICON-SI often underestimates the observed LWP.

The LWP already gives a hint on the representation of cloudy versus non-cloudy situations. To evaluate the representation of clouds in more detail, particularly their vertical distribution, we use the Cloudnet classification (Illingworth et al., 2007). The classification for the model data is done by simple thresholds. If the frozen hydrometeors are larger than $1 \times 10^{-8} \text{ kg kg}^{-1}$ the point is classified as “ice”, if the liquid water is larger than the threshold it is classified as “cloud droplets” and if both are larger as “ice & supercooled droplets”. Similarly we use the same threshold to define the “rain” and the “drizzle/rain & cloud droplets” category. The Cloudnet classification of the measurements, which is used as the reference dataset, can be seen in the first panel of Figure 3. It provides an overview of the varying situations, comprising clear sky days with a frontal system and rather fair weather conditions. Already the coarse 624 m simulation of the ICON-LOC setup (Fig. 3b) is able to reproduce this variability to a large extent. The higher resolution (78 m, Fig. 3c) seems to be beneficial mainly for its improved representation of shallow cumulus clouds at the end of the time period. As those clouds are strongly influenced by the small scales, a higher resolution improves their representation. The higher resolution also shows less precipitation events on 1 and 2 May 2013, which is also closer to the observations. The ICON-DE simulation (Fig. 3d) shows at the available days a similar representation of the daily variability, except for 2 May 2013, where the shallow cumulus clouds seem to be underestimated. We will investigate these differences further in section 5. Whereas the high ice clouds seem to be large-scale driven and are also nicely represented in the ICON-SI (DALES-SI only has warm cloud microphysics), the representation of the boundary layer clouds in the semi-idealized simulations deviates strongly from the observed conditions. The rather smooth appearance is due to the applied domain average, but additionally the semi-idealized setups emphasize the response of the small scales to the large-scale situation. The influence of mesoscales as well as a heterogeneous surface are neglected for a reduced complexity, but proves detrimental for the comparison to the observations. Figure 3 suggests that these external drivers play an important role in setting the variability. For a day-to-day comparison between column observations and simulations, the realistic simulations (ICON-DE, ICON-LOC) seem to be more generally suitable than the semi-idealized simulations.

4 Methodological biases

For the best representation of the turbulence and to facilitate comparisons with high-frequency measurements it is helpful to simulate the atmosphere at the finest possible resolution. However, limited computational resources and a desire to simulate many different cases encourages the use of coarser simulation grids. The tension between these two demands motivates a study of the resolution dependency of our simulation output. A second question that arises, is the trade-off between better resolution, and the effects of variability associated with the local conditions of the measurement site. To the extent the latter is less important it can be advantageous to use simpler and more computationally efficient semi-idealized set ups, which by virtue of their reduced overhead, would then allow simulations with higher resolution at the same cost. Finally, as a third question we ask to what extent small differences in the forcing condition the response.

4.1 Resolution Effects

4.1.1 Vertical wind

The vertical wind is fundamental for transport, and is associated with both cloud and precipitation formation. Representing its variability should thus be a metric of model fitness. In the boundary layer it mostly measures the structure of the turbulence, and

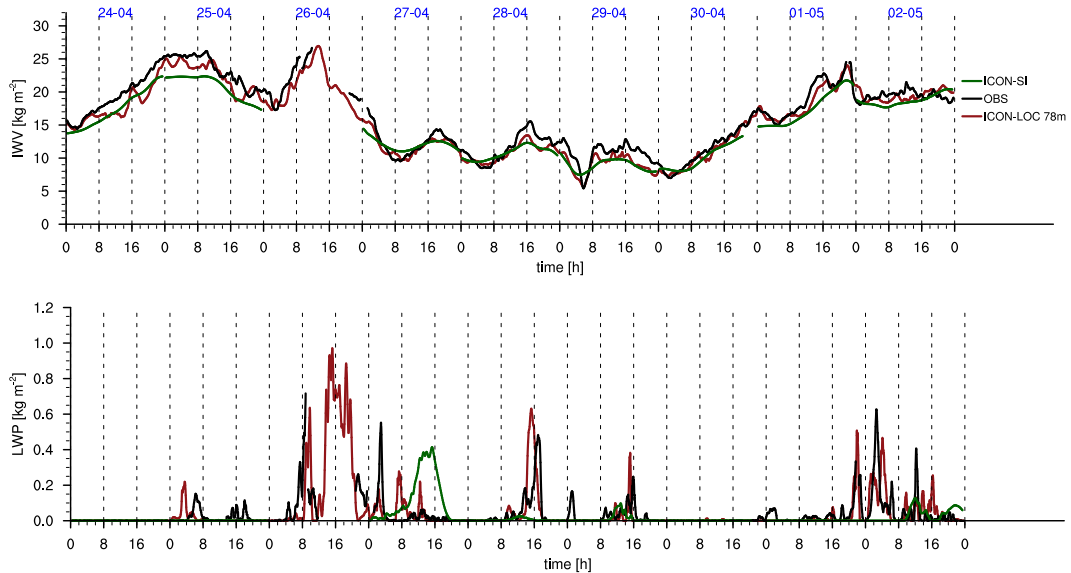


Figure 2. Time series of IWV (top) and LWP (bottom) for 29 April-2 May 2013 for JOYCE. Values are 30-min running means with observations (black), ICON-LOC with 78 m resolution (red) and ICON-SI (green).

323 above the boundary layer it will be sensitive to the development of convection. For a quan-
 324 titative idea about the effect of resolution on the vertical wind, we compare an average
 325 profile of the variance of the vertical wind from the meteogram output over all nine days
 326 for the four different ICON-LOC simulations (Fig. 4). All the simulations capture the
 327 basic structure of the vertical velocity field, but especially in the turbulent boundary layer
 328 (up to 2 km), the benefit of a higher resolution is clear. Between 2 km to 4 km only the
 329 coarsest resolution differs substantially from the finer resolution simulations, and even
 330 this difference vanishes above 5 km height. Below 2 km, differences between the two finest
 331 resolutions suggest that an even higher resolution than the 78 m will be required to fully
 332 resolve the fluctuations in the vertical velocity. On the other side, above 5 km a 624 m
 333 model resolution might already be sufficient for most studies.

334 4.1.2 Liquid water path

335 As seen in Fig. 2, LWP is more variable and probably more sensitive to resolution
 336 than IWV. For the LWP, two quantities are of interest – the mean amount of cloud wa-
 337 ter and its variance. In Fig. 5, the difference between simulated mean (variance) and ob-
 338 served mean (variance) of cloud water are shown. The left panel of Fig. 5 depicts the point
 339 to point comparison of the meteogram output and the column observations, which shows
 340 for many days an improvement with increasing resolution (e.g. for the 25 or 27 April).
 341 The shallow cumulus days (1 and 2 May) are also rather well represented, while the dis-
 342 tribution of the almost clear sky or frontal system are more sensitive and difficult to cap-
 343 ture. For this reason, days with more than 40% missing values or values smaller than
 344 1 g/m^2 are highlighted. For the point measurements, we are still left with the question
 345 of how much of the differences between model and observations are due to hits or misses.
 346 To answer this question, we selected a sub-region (see Fig. 1), which is included in each
 347 domain of the ICON-LOC and ICON-DE and compared the domain mean of LWP for
 348 the different resolutions (Fig. 5, right). For the domain means, the improvement by in-
 349 creasing resolution can be seen in the tendency for each setup to reduce the differences
 350 in mean LWP and in the variance of LWP, i.e. the symbols in Fig. 5 (right) denoting higher-

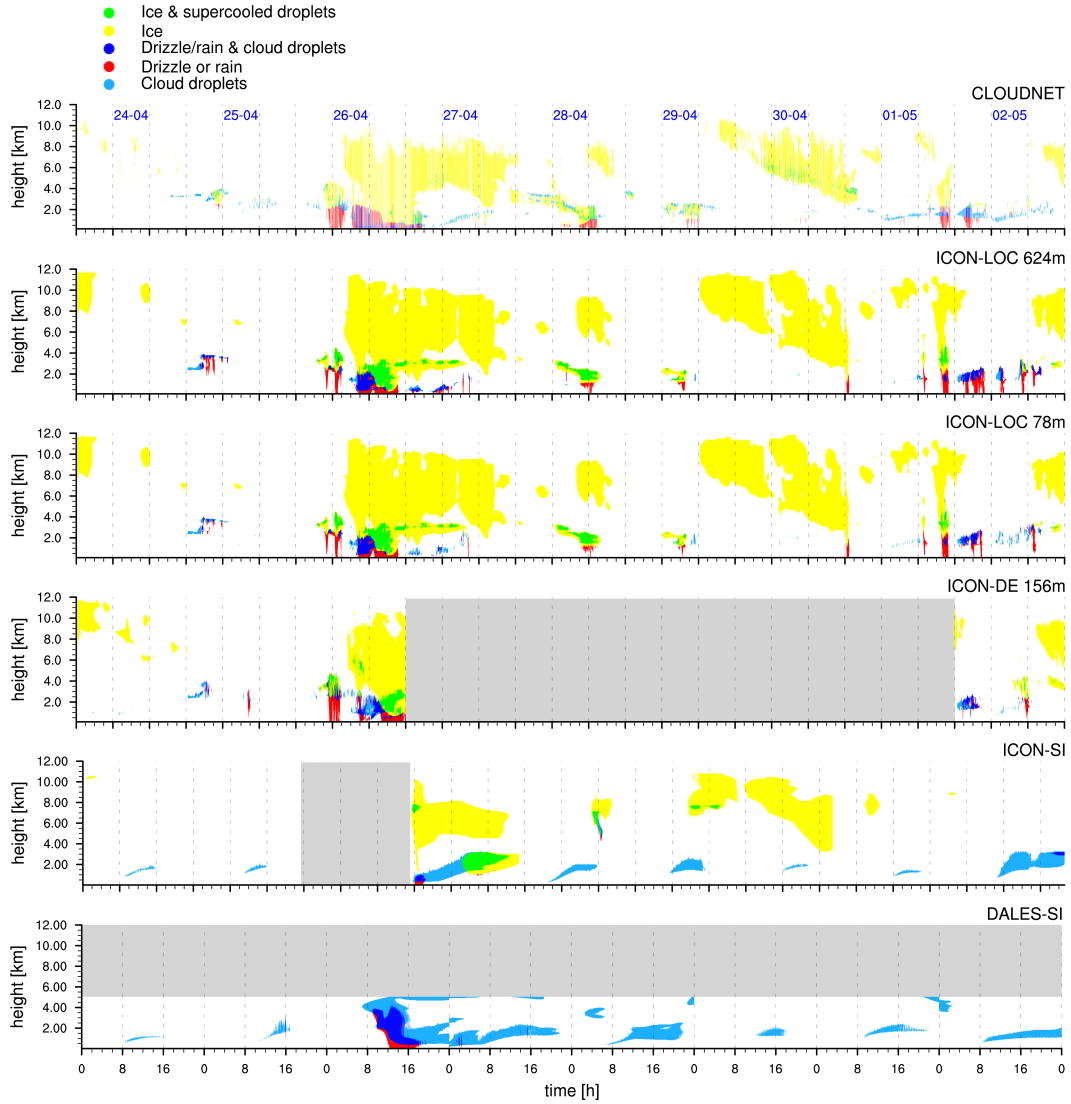


Figure 3. CLOUDNET classification at JOYCE for 26 April to 2 May 2013 and hydrometeor classification for varying model setups: ICON-LOC with 624 m and 78 m resolution, ICON-DE, ICON-SI and DALES-SI (from top to bottom). Model classifications are calculated based on a threshold of $1.0 \times 10^{-8} \text{ kg kg}^{-1}$ for the different hydrometeors. Grey color indicates missing simulation days.

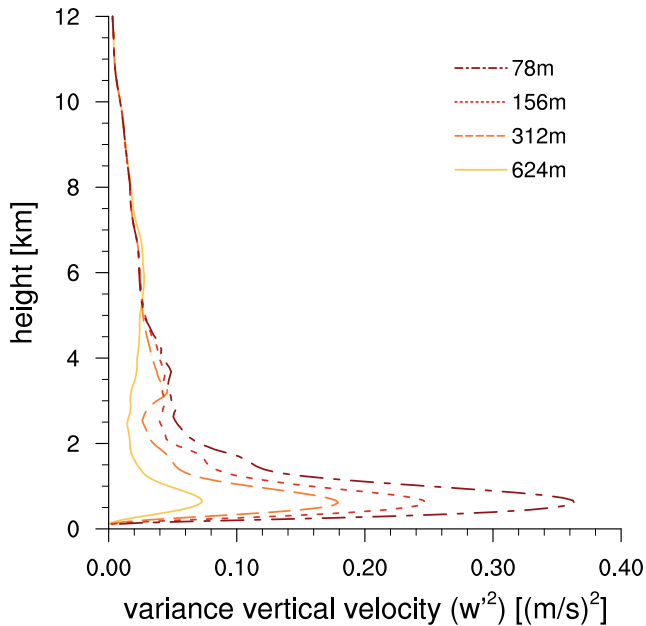


Figure 4. Mean variance of vertical wind from ICON-LOC meteogram output for different resolutions. The variance is calculated for each day and then averaged over all nine days (29 April-2 May 2013).

351 resolution are shifted progressively towards the origin (esp. 29 April or 1 May). An inter-
 352 esting feature can be seen at the right panel for the ICON-LOC at the 2nd of May,
 353 where the difference in the mean LWP is decreasing, but the difference in the variance
 354 of LWP is increasing. In general, the symbols on the left plot are rather clustered around
 355 the y -axis, while the symbols on the right plot are closer to the x -axis. This supports
 356 the expected improved representation of the variability of LWP by applying the meteogram
 357 output vs. an improved representation of the general amount by taking the domain mean.

358 4.2 Representativeness of column observations

359 One important question for column observations is always how representative these
 360 observations are for the surrounding region. By including surface heterogeneity and mesoscale
 361 circulations, the model has the potential to tackle this question. As our main interest
 362 are clouds and their representation in the model, we continue analyzing the represen-
 363 tativeness of LWP, as might be observed within a single column, for a larger domain, and
 364 vice versa. The question is how well the LWP distribution at one point compares to the
 365 LWP distributions of the neighboring points. To answer this, we need a measure to com-
 366 pare different density functions. For this we use the Hellinger distance H , which is de-
 367 fined as:

$$H(P, Q) = \frac{1}{\sqrt{2}} \sqrt{\sum_{i=1}^k (\sqrt{p_i} - \sqrt{q_i})^2},$$

368 where $P = (p_1, \dots, p_k)$ and $Q = (q_1, \dots, q_k)$ are two different discrete probability dis-
 369 tributions. $H(P, Q) = 0$ implies that the distributions are identical, while $H(P, Q) =$
 370 1 stands for completely disjunct distributions.

371 We calculated H for each day and for each grid cell in a sub-region, that is con-
 372 tained in all 4 nests, by comparing the LWP distribution of a given grid-column to the
 373 reference grid-column covering the observational site. For each day the probability of the

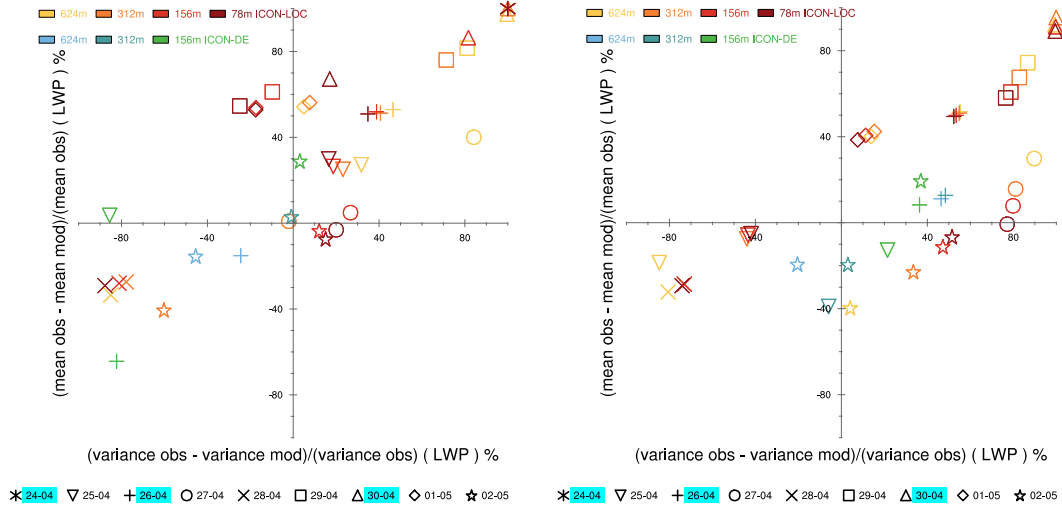


Figure 5. Percentage difference of mean LWP and variance of LWP between simulations and observations at JOYCE for each day (26 April - 2 May 2013). Model data are the meteogram output (9-s resolution, left) and the domain mean (10-min resolution, right). The colors indicate the different model setup, the symbols the different days. Days with more than 40% of missing values or values smaller than 1 g/m^2 are highlighted with blue.

374 given grid column and the reference column is constructed from the temporal data, as
 375 if each measurement were an independent sample. Figure 6 shows H for each grid col-
 376 umn averaged over all nine days. By definition $H = 0$ at the reference column. Even
 377 though the average is presented, all resolutions show a similarly distinct regional pat-
 378 tern. Higher values are apparent to the East, and there also appears wind-aligned (roughly
 379 east-west oriented) structures of small and large H . This points out the importance of
 380 taking the surface and also the meteorological conditions (e.g. wind direction) into ac-
 381 count, as they are most likely dominating the pattern. While our statistic is still lim-
 382 ited, the setup could be used to determine a region for which the column observations
 383 are still representative. This likely depends on the meteorological regime, and for this
 384 a longer time period of simulations would be beneficial. Especially in regions dominated
 385 by topography or surface features (like the open-pit mine a few kilometers East of the
 386 observation site) such a study could be informative for discussions of where to set up cer-
 387 tain observing systems. Another application could be the investigation of changes in the
 388 pattern due to surface changes, created intentionally, e.g., the mining activities, or by
 389 climate change.

390 Figure 7 shows the relative bias of the domain average of LWP with respect to the
 391 observed mean and the corresponding domain mean of H . The domain mean of H is used
 392 as a measure for the similarity between the LWP density function at the grid-cell of the
 393 observations and the surrounding. For H , we see two different clusters: one around $H \approx$
 394 0.25 and one with $H \approx 0.45$. Additionally, there is a tendency towards larger H for larger
 395 mean LWP differences. So in cases where the bias is large, we also have a higher LWP
 396 variability within the domain and the point-to-point comparison is less representative.

397 Figure 7 as well as Fig. 5 additionally show that the spread of the results for the
 398 different resolutions of ICON-DE is larger than for the different resolutions of ICON-LOC.
 399 This can most likely be explained by the more constrained forcing and setting for the
 400 small domains, compared to the large domains of the ICON-DE which allow for the rep-
 401 resentation of a wider range of scales. This can be beneficial as the mesoscale circula-

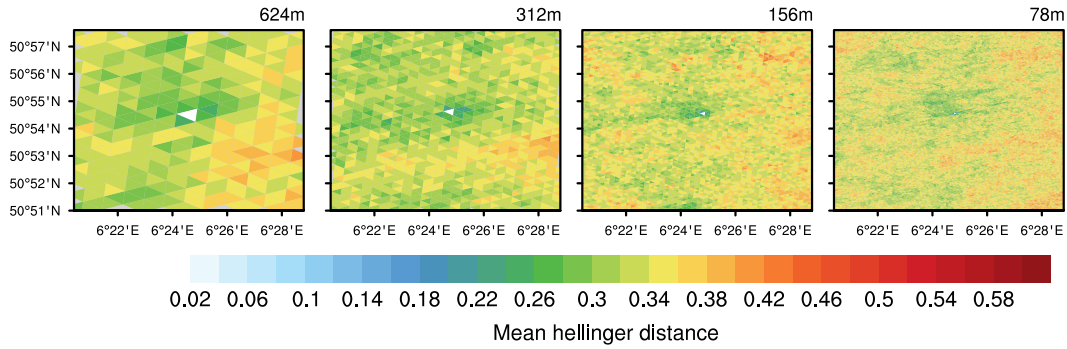


Figure 6. Mean Hellinger distance, H , with respect to the central cell closest to the location of JOYCE. The Hellinger distance has been calculated for each day (26 April - 2 May 2013) and then averaged over all 9 days.

402 tions have more time to evolve, but the more realistic setting, with rich mesoscale vari-
 403 ability, also poses additional challenges to the comparison with point measurements.

404 4.3 Influence of the forcing dataset

405 An important question for limited area simulations (including regional climate mod-
 406 els) is always the dependency on the large-scale forcing (e.g. Warner et al., 1997; K oltzow
 407 et al., 2011; Laprise et al., 2012). Especially the semi-idealized LES are known to de-
 408 pend strongly on the large-scale forcing (e.g. W. I. Gustafson et al., 2020). In this sec-
 409 tion, we will show that one advantage of the forcing at the open boundaries is a reduced
 410 dependency on the large-scale forcing. To do so we compare the previous ICON-LOC
 411 simulations forced with COSMO-DE with an additional set of ICON-LOC simulations
 412 forced with IFS data.

413 Figure 8 shows the hydrometeor classification for the location of JOYCE from the
 414 COSMO-DE and the IFS, the two models used to create the local forcings. The two fore-
 415 cast systems produce a similar picture of the synoptic situation (cf. Fig. 3a), something
 416 also shown by Barthlott and Hoose (2015), but differ substantially in their details. These
 417 differences are most pronounced in the lower atmosphere (below 4 km) where the IFS
 418 forcing supports the development of more liquid and mixed-phase clouds and precipi-
 419 tation in the lower boundary layer as compared to both COSMO-DE and the Cloudnet
 420 observations. The better representation of the lower atmosphere by the COSMO-DE sim-
 421 ulations is, by virtue of its much finer resolution to be expected. Our point here is not
 422 which system is better, but to then ask to what extent the LEM simulations inherit the
 423 differences apparent in the forcing data sets.

424 Despite differences in the host models used to produce the forcing datasets, the re-
 425 sults of the ICON-LOC simulations forced with COSMO-DE and IFS, respectively (Fig. 9),
 426 compare very well to each other. Thus, the differences in the forcing seem to be reduced
 427 through the high-resolution setup. The simulations forced by the IFS seem to have an
 428 slightly enhanced precipitation frequency, suggesting that the higher amount of clouds
 429 and precipitation in the IFS itself, may be partially forced. Past work has shown, in other
 430 context, that large differences can occur, as shown for an example in case of Arctic mixed-
 431 phased clouds (Schemann & Ebell, 2020). We speculate that this reflects a reduced role
 432 for surface driven turbulence and the complexity of mixed-phase clouds in those situa-
 433 tions. In the present context of early summer convection over land, the results seem less
 434 sensitive to the forcing. The more realistic set-ups, which admit a larger role for the mesoscale,
 435 may also make the results less sensitive to the large-scale forcing.

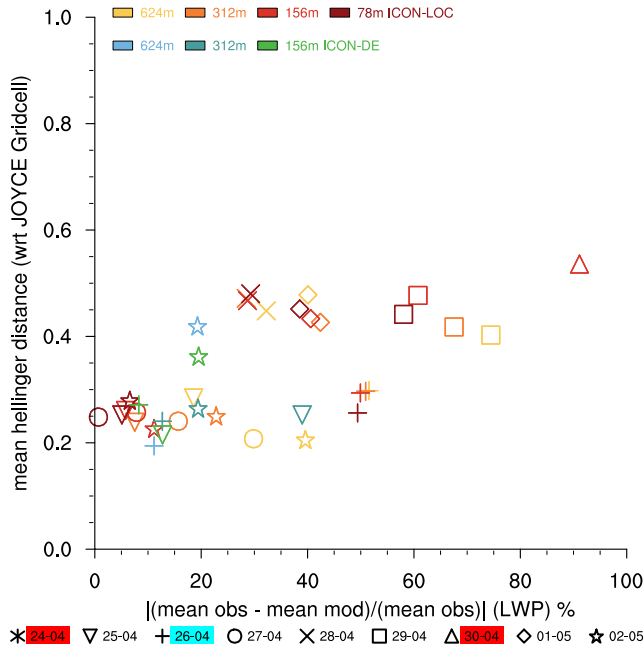


Figure 7. Absolute value of the difference (%) of domain mean LWP between simulations and observations at JOYCE and domain mean Hellinger distance for each day (26 April - 2 May 2013). Red indicates the two days without observed liquid clouds, and cyan the frontal day, which includes a large uncertainty in the measurements.

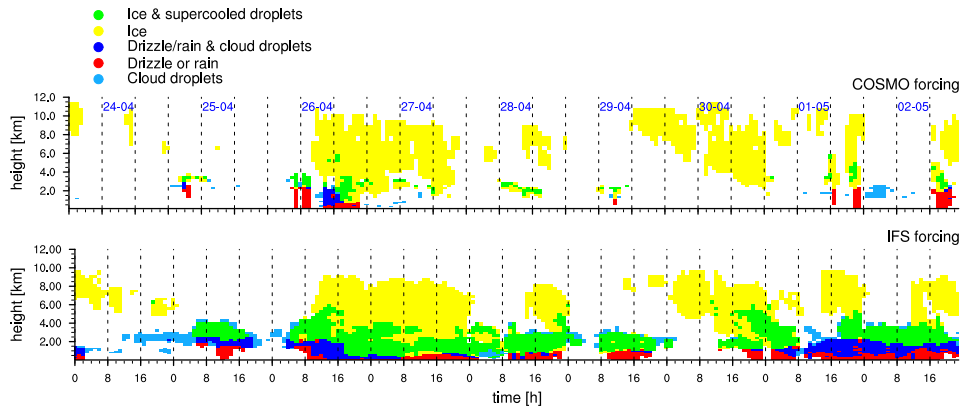


Figure 8. Hydrometeor classification at the location of JOYCE for 26 April to 2 May 2013 from the COSMO-DE forcing data (hourly data, top) and the IFS forcing data (hourly data, bottom). Model classifications are calculated based on a threshold of $1 \times 10^{-8} \text{ kg kg}^{-1}$ for the different hydrometeors.

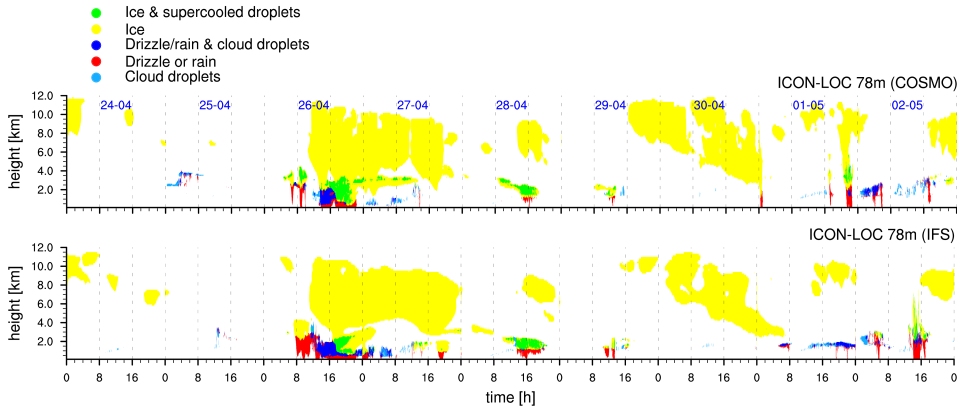


Figure 9. Hydrometeor classification at the location of JOYCE for 26 April to 2 May 2013 from ICON-LOC at 78 m resolution forced with COSMO-DE (top) and IFS (bottom). Model classifications are calculated based on a threshold of $1 \times 10^{-8} \text{ kg kg}^{-1}$ for the different hydrometeors.

436 5 Case study - Zooming in on 2 May 2013

437 While large-scale forcing always plays a role, especially idealized LES are useful for
 438 highlighting particular features in a general way - e.g. shallow cumulus convection. In-
 439 deed, that is the purpose of the idealization. For this reason, we will focus in this sec-
 440 tion on 2 May 2013 where a convectively driven boundary-layer development topped with
 441 afternoon shallow cumulus was observed. This situation is typical of the type of situa-
 442 tion often studied with LES, and the enhanced homogeneity is better suited for the ap-
 443 plication of ICON-SI and DALES-SI, allowing them to be compared to the more realis-
 444 tic set-ups in the most favorable manner possible. Our analysis focuses on the devel-
 445 opment of the cloud field, and at the end explores to what extent differences between
 446 the ICON-LOC and ICON-SI/DALES-SI can be explained by the influence of topogra-
 447 phy alone.

448 5.1 Hydrometeor classification

449 A more detailed assessment of the cloud classification of 2 May 2013 (Fig. 10) shows
 450 that all model setups can capture the typical shallow cumulus clouds during mid-day.
 451 The cloud classification based on domain averages – for the semi-idealized (Fig. 10e,f)
 452 as well as for the realistic setup (Fig. 10d) – accentuates the cloud features. This is par-
 453 ticularly pronounced for the case of the boundary layer cloud development; the semi-idealized
 454 cases emphasize the canonical development of the convective boundary layer with a grow-
 455 ing cloud layer between approximately 12 noon and 4 pm (cf., Brown et al., 2002). In the
 456 meteogram output of the realistic setups (Fig. 10a,b), the clouds are more scattered through-
 457 out the day and their representation seems to improve with resolution. The 78 m sim-
 458 ulation with the ICON-LOC shows a cloud structure that is most similar to the observed
 459 clouds – suggesting that indeed as more detail is added to the turbulent flow and the sur-
 460 face representation, the simulations more closely approximate the observations.

461 Also the clouds near the surface in the morning are apparent in the more realis-
 462 tic simulations, but either not apparent or distorted by the semi-idealized framework.
 463 Wind lidar measurements (not shown) suggest these to be decoupled from the surface.
 464 The absence of these clouds in the ICON-SI and their prevalence in DALES-SI suggests
 465 that these clouds are likely driven by differences in the large-scale flow, as DALES-SI is
 466 forced by the IFS and the ICONS-SI by COSMO-DE.

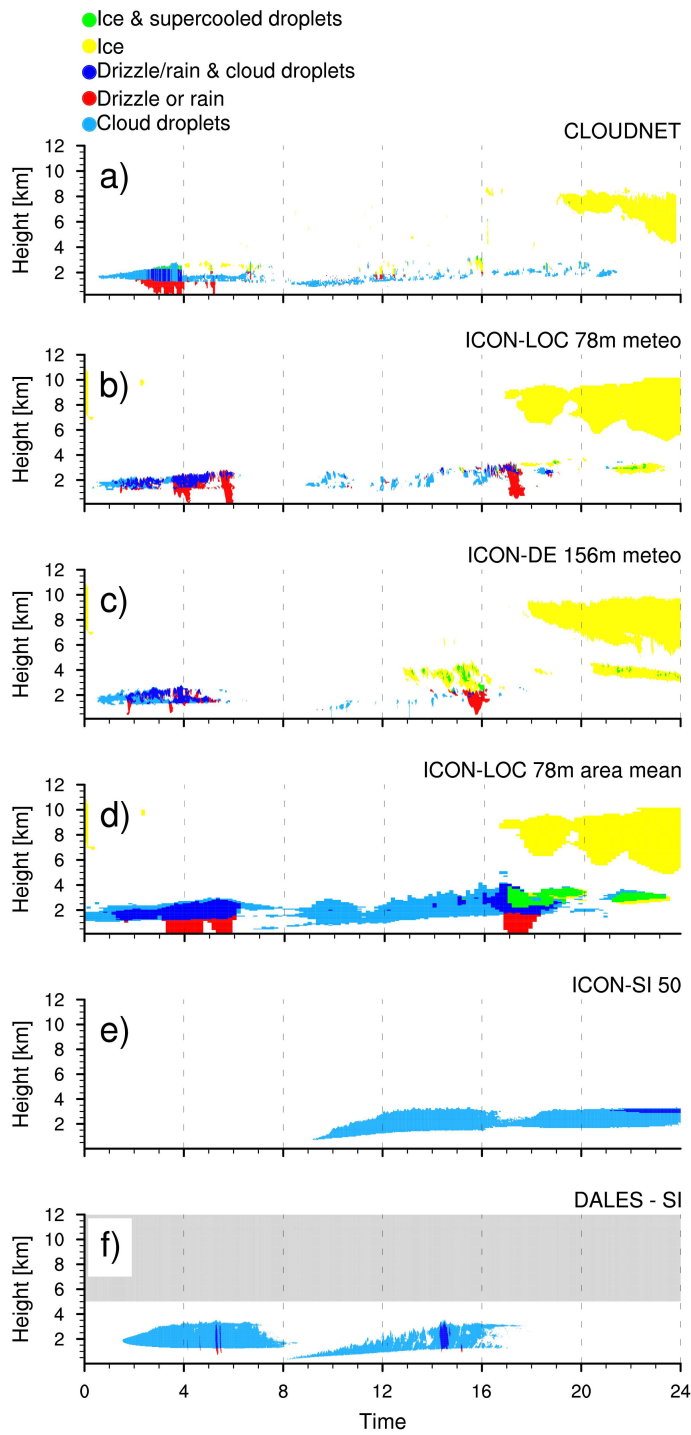


Figure 10. Hydrometeor classification at JOYCE for 2 May 2013. a) CLOUDNET. Meteorogram output of b) ICON-LOC with 78 m resolution and c) ICON-DE. Results based on domain mean profiles of d) ICON-LOC with 78 m resolution, e) ICON-SI and f) DALES-SI. Model classifications are calculated based on a threshold of $1 \times 10^{-8} \text{ kg kg}^{-1}$ for the different hydrometeors.

467 For the ice clouds on 2 May 2013, more systematic differences occur. In the very
 468 early morning, all realistic simulations with COSMO-DE forcing (Fig. 10b-d) show some
 469 ice clouds between 7 and 11 km height which are not seen in the observations. These sim-
 470 ulated ice clouds are related to ice clouds which have been observed late in the evening
 471 on the previous day and linger longer in the simulations than they did in reality. The
 472 high ice cloud seen by the observations between 7 pm and midnight on 2 May 2013 is
 473 well captured by the realistic setups but missed by the semi-idealized models. This is
 474 reasonable for DALES-SI as it was run without ice-microphysics, but ICON-SI uses the
 475 same 2-moment microphysics scheme as ICON-LOC. Probably this ice cloud is due to
 476 inflow at the domain boundaries and not captured by the mean nudging profile. Addi-
 477 tionally, all realistic setups have ice/mixed-phase clouds at a height of around 4 km in
 478 the afternoon, which are not seen by the observations. These simulated ice clouds might
 479 trigger the precipitation development around 4 and 5 pm in ICON-LOC and ICON-DE
 480 which is not observed either. The ICON-DE setup produces even more ice clouds than
 481 the ICON-LOC, which leads especially for the coarse resolution to even more precipi-
 482 tation.

483 Based on these analyses, the early boundary layer clouds are probably due to in-
 484 flow into the boundary, the mid-day clouds due to typical boundary layer development
 485 and the afternoon clouds due to the influence by the topography which will be analyzed
 486 in more detail in Sec. 5.3.

487 5.2 Horizontal LWP variability

488 As seen in the previous section, it is difficult to establish if a disagreement between
 489 observations and simulations is due to physical reasons or due to a displacement in space
 490 or time. For liquid clouds, the assessment of the two-dimensional output of LWP can pro-
 491 vide some insights here. We thus selected a sub-domain that is included in all domains
 492 of the ICON-LOC and ICON-DE setups and counted all time steps with LWP greater
 493 than 1 g/m^2 between 11 am and 1 pm on 2 May 2013. Figure 11 shows the occurrence
 494 of liquid clouds in the selected domain for ICON-LOC (156 and 78 m), ICON-DE and
 495 ICON-SI. Indeed, the ICON-LOC simulations show clearly more liquid cloud cases than
 496 the ICON-DE 156 m simulations. However, by far the most liquid clouds are counted for
 497 the ICON-SI simulation. For the ICON-LOC simulations, the amount of clouds around
 498 JOYCE (central point) is increasing with increasing resolution. The two-dimensional pic-
 499 ture shows that the underestimation of the mid-day boundary layer clouds on 2 May 2013
 500 for ICON-DE at 156 m resolution (Fig. 10) is not simply due to a misplacement of the
 501 clouds. Overall the comparison gives the impression, that at least for this case, enhanced
 502 spatial variability reduces cloudiness.

503 5.3 Topography experiment

504 To test the hypothesis that the afternoon clouds are less synoptically, and more to-
 505 pographically, driven, we performed a sensitivity experiment with ICON-LOC at 624 m
 506 resolution where the topography (Fig. 1, middle) has been removed. For this, the sur-
 507 face height was set to 110 m in all grid cells which is approximately the surface height
 508 at JOYCE. This reduces the influence of the topography, even though some trace of it
 509 will still be present in the forcing, e.g., pressure profiles or humidity gradients. The com-
 510 parison of the hydrometeor classification between the runs with and without topogra-
 511 phy (Fig. 12) supports our hypothesis that the topography mainly influences the after-
 512 noon boundary layer clouds. While the morning and mid-day clouds are almost not at
 513 all influenced by the change in the topography, the afternoon clouds disappear in the model
 514 run without topography. The result is a little surprising, because the semi-idealized frame-
 515 works also lack topography but have a very strong development of fair-weather cumu-
 516 lus in the afternoon. We suspect that the presence of topography either contributes to
 517 the moistening or deepening of the boundary layer in ways that support cloud develop-

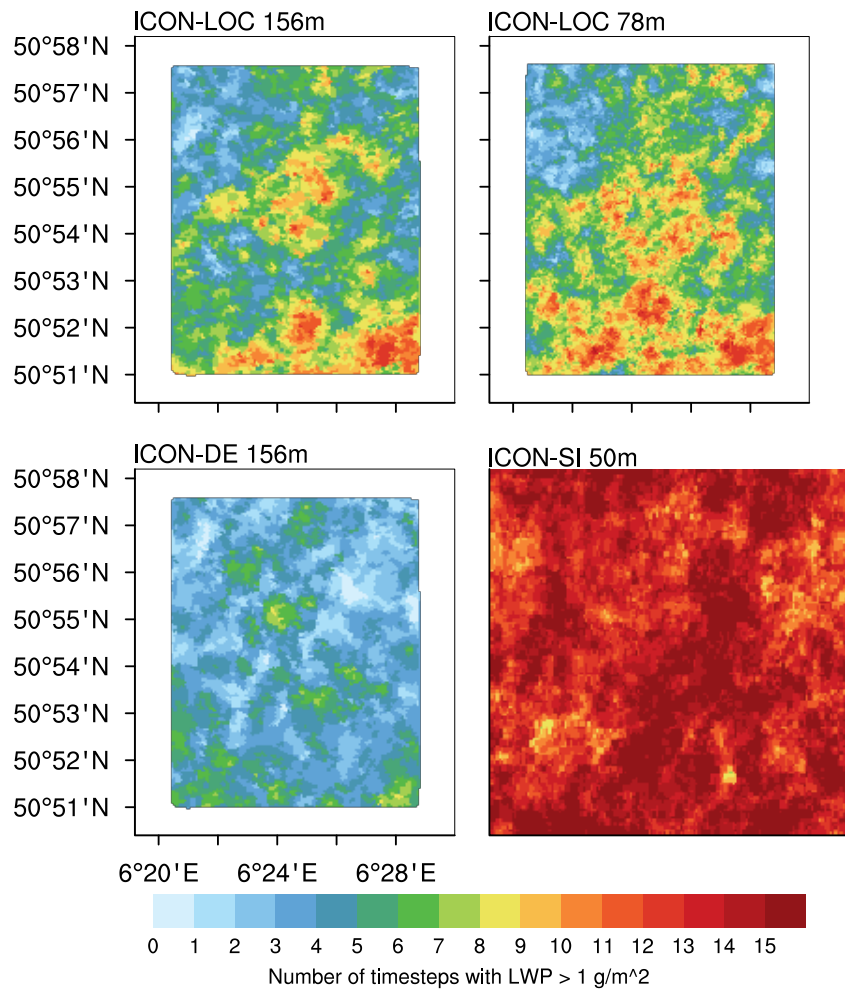


Figure 11. Number of timesteps per gridcell with LWP > 1 g/m² between 11 am and 2 pm (18 timesteps) for selected model setups.

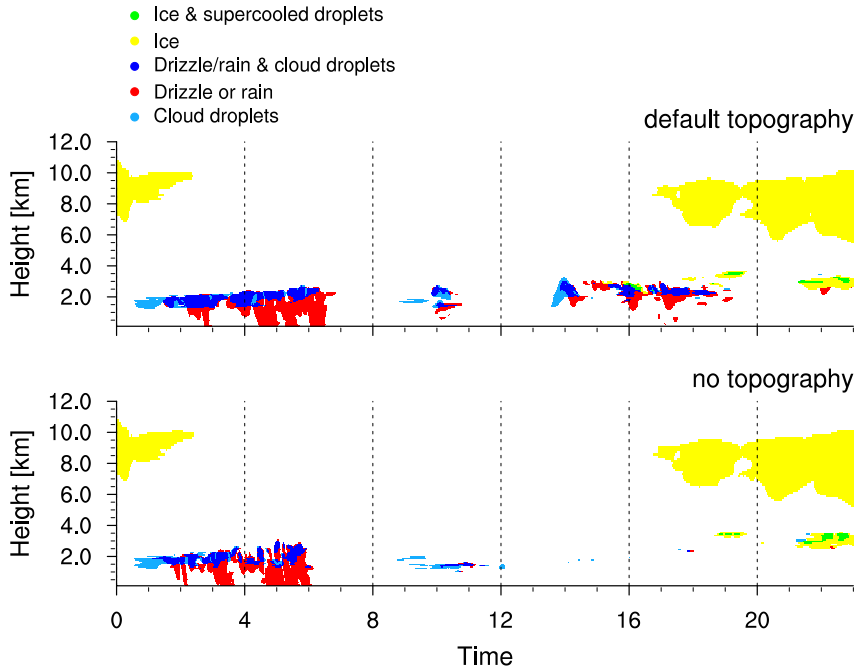


Figure 12. Hydrometeor classification at JOYCE for 2 May 2013 for ICON-LOC with 624 m resolution and a) the default topography and b) no explicit topography. Model classifications are calculated based on a threshold of $1 \times 10^{-8} \text{ kg kg}^{-1}$ for the different hydrometeors.

518 ment. Further experiments, not shown, but with less extreme changes in topography sup-
 519 port this finding. In the realistic configuration of the model cloudiness increases with the
 520 strength of the topographic forcing. In some ways this finding is counter to what we found
 521 previously, whereby the inclusion of mesoscale variability as we progressively transition
 522 from the semi-idealized to the large-domain ICON-DE simulations (e.g., Fig. 11), led to
 523 a reduction in cloudiness. It suggests that the enhanced cloudiness of the semi-idealized
 524 simulations is if anything understated by virtue of their missing topographic forcing.

525 6 Summary and Conclusion

526 With the ongoing evolution of observational and computational capabilities, the
 527 interest to compare high-resolution simulations and observations on a day-to-day basis
 528 has grown (e.g. van Laar et al., 2019; W. I. Gustafson et al., 2020). Such comparisons
 529 are difficult if the models exhibit large biases in the representation of the synoptic set-
 530 ting. In this study, we compared three different approaches for bringing models together
 531 with observations from a fixed ground location: the traditional semi-idealized LES (ICON-
 532 SI, DALES-SI), defined as simulations without externally imposed heterogeneity, neither
 533 at the surface, nor in the forcing, the more realistic setup on a very large domain (ICON-
 534 DE), and the realistic setup on a small and constrained domain (ICON-LOC). By an-
 535 alyzing a 9-day period in spring 2013 (26 April - 2 May 2013) in Germany, we could point
 536 out advantages and disadvantages of the various setups.

537 The semi-idealized LES are designed to emphasize particular flow features, this leads
 538 to a distortion – usually by over-emphasis – of those features as compared to what is ob-
 539 served. Especially for the shallow cumulus days, they produce, as expected, cumulus clouds
 540 on top of a well-mixed boundary layer. These setups may be suitable to analyze processes

541 but are less well adapted to assessing their compatibility with observations, particularly
 542 over land sites with even modest heterogeneity.

543 The more realistic setups that take these effects into account by incorporating lat-
 544 eral boundary conditions from NWP models and a heterogeneous surface capture the
 545 different atmospheric conditions of the 9-day period: they show a reasonable represen-
 546 tation of the general cloud structure, including height, time and phase. Especially for
 547 the days when small-scale processes are more important – as the mentioned shallow-cumulus
 548 days – higher resolution and smaller domains are beneficial for a better cloud represen-
 549 tation. In initiating this study we expected that the very large domain of the ICON-DE
 550 would lead to the best results, due to the possibility of freely evolving meso-scale pro-
 551 cesses. As we learned, this free evolution causes some drawbacks. It seems that a more
 552 constrained and smaller domain allows for a tighter control on the synoptic situation,
 553 and may be the preferred choice if the aim is a better comparison to observations with
 554 point measurements from the surface.

555 Another advantage of the small domain is the relatively low computational demand,
 556 which makes it possible to run enough simulations for a statistical analysis and to in-
 557 vestigate sensitivities by additional experiments. We shortly touched the issue of rep-
 558 resentativeness, which is a longstanding question for column observations and also gains
 559 importance due to specific output strategies, such as the meteogram output used in much
 560 of our analysis. A small domain setup as the ICON-LOC provides a reasonable repre-
 561 sentation of the cloud structure and can be used to tackle the question of representative-
 562 ness in the future by using long-term simulations and e.g. analyzing measures as the Hellinger
 563 distance to compare distributions of atmospheric variables at different points in space
 564 and time.

565 We highlighted the importance of including a realistic topography in the high-resolution
 566 simulations by means of a sensitivity study. Such model experiments are not limited to
 567 changes in topography but also can be applied to changes of other surface properties,
 568 e.g. land cover, which can either be natural or man-made. The potential of the model
 569 to characterize the impact of such changes will play a large role in future research.

570 By comparing three different model setups with column observations, we showed
 571 the advantages and disadvantages of the different setups. An encouraging aspect of the
 572 exercise was that as more 'realism' was added, either by the inclusion of finer scales of
 573 turbulence or through more realistic boundary conditions, the simulations more closely
 574 approximated the observations. Simulations over a realistic domain localized around the
 575 observational site appear to be a computationally expedient and effective way to bring
 576 modelling and observations together to develop understanding the physics underpinning
 577 how condensate forms and is distributed within atmospheric circulations.

578 **Acknowledgments**

579 The project HD(CP)2(High Definition Clouds and Precipitation for advancing Climate
 580 Prediction) was funded by the German Federal Ministry of Education and Research within
 581 the framework programme "Research for Sustainable Development (FONA)" under the
 582 numbers 01LK1501 – 01LK1508A and 01LK1509A. The authors gratefully acknowledge
 583 the computing time granted on the supercomputer MISTRAL at Deutsches Klimarechen-
 584 zentrum GmbH (DKRZ) through its Scientific Steering Committee (WLA). Data were
 585 provided by Jülich Observatory for Cloud Evolution (JOYCE-CF), a core facility funded
 586 by Deutsche Forschungsgemeinschaft via grant DFG LO 901/7-1. JOYCE-CF is an in-
 587 tegral part of CPEX-Lab, a competence center of the Geoverbund ABC/J. The ICON-
 588 LOC simulations will be stored (by acceptance) at the long-term archive of the German
 589 Climate Computing Center (DKRZ; <http://cera-www.dkrz.de>).

References

590

- 591 Baldauf, M., Seifert, A., Foerstner, J., Majewski, D., Raschendorfer, M., & Rein-
 592 hardt, T. (2011). Operational convective-scale numerical weather prediction
 593 with the COSMO model: Description and sensitivities. *Mon. Wea. Rev.*, *139*,
 594 3887 – 3905. doi: 10.1175/MWR-D-10-05013.1
- 595 Barthlott, C., & Hoose, C. (2015). Spatial and temporal variability of clouds
 596 and precipitation over Germany: multiscale simulations across the "gray
 597 zone". *Atmospheric Chemistry and Physics*, *15*(21), 12361–12384. Re-
 598 trieved from <https://www.atmos-chem-phys.net/15/12361/2015/> doi:
 599 10.5194/acp-15-12361-2015
- 600 Bony, S., Colman, R., Kattsov, V. M., Allan, R. P., Bretherton, C. S., Dufresne, J.-
 601 L., ... Webb, M. J. (2006). How well do we understand and evaluate climate
 602 change feedback processes? *Journal of Climate*, *19*(15), 3445–3482. Retrieved
 603 from <https://doi.org/10.1175/JCLI3819.1> doi: 10.1175/JCLI3819.1
- 604 Boucher, O., Randall, D., Artaxo, P., Bretherton, C., Feingold, G., Forster, P., ...
 605 Zhang, X. Y. (2013). Clouds and aerosols. In T. F. Stocker et al. (Eds.),
 606 *Climate change 2013: The physical science basis. contribution of working*
 607 *group i to the fifth assessment report of the intergovernmental panel on climate*
 608 *change* (pp. 571–657). Cambridge, UK: Cambridge University Press. doi:
 609 10.1017/CBO9781107415324.016
- 610 Brown, A. R., Cederwall, R. T., Chlond, A., Duynkerke, P. G., Golaz, J.-C.,
 611 Khairoutdinov, M., ... Stevens, B. (2002). Large-eddy simulation of
 612 the diurnal cycle of shallow cumulus convection over land. *Quarterly*
 613 *Journal of the Royal Meteorological Society*, *128*(582), 1075–1093. doi:
 614 10.1256/003590002320373210
- 615 Browning, K. A., Jonas, P. R., Kershaw, R., Manton, M., Mason, P. J., Miller, M.,
 616 ... Simpson, J. (1993, March). The GEWEX cloud system study (GCSS).
 617 *Bulletin of the American Meteorological Society*, *74*(3), 387–399.
- 618 Cess, R. D., Potter, G. L., Blanchet, J. P., Boer, G. J., Del Genio, A. D., Déqué,
 619 M., ... Zhang, M.-H. (1990). Intercomparison and interpretation of cli-
 620 mate feedback processes in 19 atmospheric general circulation models. *Jour-
 621 nal of Geophysical Research: Atmospheres*, *95*(D10), 16601–16615. doi:
 622 10.1029/JD095iD10p16601
- 623 Chow, F. K., Weigel, A. P., Street, R. L., Rotach, M. W., & Xue, M. (2006, Janu-
 624 ary). High-Resolution Large-Eddy Simulations of Flow in a Steep Alpine
 625 Valley. Part I: Methodology, Verification, and Sensitivity Experiments. *J. Of*
 626 *Appl. Meteorol.*, *45*(1), 63–86.
- 627 Dipankar, A., Stevens, B., Heinze, R., Moseley, C., Zängl, G., Giorgetta, M., & Br-
 628 dar, S. (2015). Large eddy simulation using the general circulation model
 629 ICON. *Journal of Advances in Modeling Earth Systems*, *7*(3), 963–986. doi:
 630 10.1002/2015MS000431
- 631 Gustafson, W., Vogelmann, A., Cheng, X., Dumas, K., Endo, S., Johnson, K., ...
 632 Xiao, H. (2019). *Description of the LASSO Data Bundles Product. DOE*
 633 *Atmospheric Radiation Measurement (ARM) user facility* (Tech. Rep.).
 634 DOE/SC-ARM-TR-216. doi: 10.2172/1469590
- 635 Gustafson, W. I., Vogelmann, A. M., Li, Z., Cheng, X., Dumas, K. K., Endo, S.,
 636 ... Xiao, H. (2020). The Large-Eddy Simulation (LES) Atmospheric Radi-
 637 ation Measurement (ARM) Symbiotic Simulation and Observation (LASSO)
 638 Activity for Continental Shallow Convection. *Bulletin of the American Meteoro-*
 639 *logical Society*, *101*(4), E462–E479. doi: 10.1175/BAMS-D-19-0065.1
- 640 Heinze, R., Dipankar, A., Henken, C. C., Moseley, C., Sourdeval, O., Trömel, S., ...
 641 Quaas, J. (2017). Large-eddy simulations over Germany using ICON: a com-
 642 prehensive evaluation. *Quarterly Journal of the Royal Meteorological Society*,
 643 *143*(702), 69–100. doi: 10.1002/qj.2947
- 644 Heinze, R., Moseley, C., Böske, L. N., Muppa, S. K., Maurer, V., Raasch, S., &

- 645 Stevens, B. (2017). Evaluation of large-eddy simulations forced with
 646 mesoscale model output for a multi-week period during a measurement
 647 campaign. *Atmospheric Chemistry and Physics*, *17*(11), 7083–7109. doi:
 648 10.5194/acp-17-7083-2017
- 649 Heus, T., van Heerwaarden, C. C., Jonker, H. J. J., Pier Siebesma, A., Axelsen,
 650 S., van den Dries, K., ... Vilà-Guerau de Arellano, J. (2010). Formulation
 651 of the Dutch Atmospheric Large-Eddy Simulation (DALES) and overview
 652 of its applications. *Geoscientific Model Development*, *3*(2), 415–444. doi:
 653 10.5194/gmd-3-415-2010
- 654 Holloway, C. E., Petch, J. C., Beare, R. J., Bechtold, P., Craig, G. C., Derbyshire,
 655 S. H., ... Woolnough, S. J. (2014). Understanding and representing atmo-
 656 spheric convection across scales: recommendations from the meeting held at
 657 dartington hall, devon, uk, 28–30 january 2013. *Atmospheric Science Letters*,
 658 *15*(4), 348-353. Retrieved from [https://rmets.onlinelibrary.wiley.com/](https://rmets.onlinelibrary.wiley.com/doi/abs/10.1002/asl2.508)
 659 [doi/abs/10.1002/asl2.508](https://rmets.onlinelibrary.wiley.com/doi/abs/10.1002/asl2.508) doi: 10.1002/asl2.508
- 660 Illingworth, A. J., Hogan, R. J., O'Connor, E., Bouniol, D., Brooks, M. E., De-
 661 lanoé, J., ... Wrench, C. L. (2007, 06). Cloudnet: Continuous Evaluation
 662 of Cloud Profiles in Seven Operational Models Using Ground-Based Observa-
 663 tions. *Bulletin of the American Meteorological Society*, *88*(6), 883-898. doi:
 664 10.1175/BAMS-88-6-883
- 665 Költzow, M., Iversen, T., & Haugen, J. (2011). The importance of lateral bound-
 666 aries, surface forcing and choice of domain size for dynamical downscaling of
 667 global climate simulations. *Atmosphere*, *2*, 67-95.
- 668 Laprise, R., Kornic, D., Rapaic, M., Separovic, L., Leduc, M., Nikiema, O., ...
 669 Biner, S. (2012). Considerations of domain size and large-scale driving for
 670 nested regional climate models: Impact on internal variability and ability at
 671 developing small-scale details. climate change. Wien: Springer-Verlag. doi:
 672 10.1007/978-3-7091-0973-1_14
- 673 Löhnert, U., Schween, J. H., Acquistapace, C., Ebell, K., Maahn, M., Barrera-
 674 Verdejo, M., ... Crewell, S. (2015). JOYCE: Jülich Observatory for Cloud
 675 Evolution. *Bulletin of the American Meteorological Society*, *96*(7), 1157-1174.
 676 doi: 10.1175/BAMS-D-14-00105.1
- 677 Macke, A., Seifert, P., Baars, H., Barthlott, C., Beekmans, C., Behrendt, A., ...
 678 Xie, X. (2017). The HD(CP)² Observational Prototype Experiment (HOPE)
 679 – an overview. *Atmospheric Chemistry and Physics*, *17*(7), 4887–4914. doi:
 680 10.5194/acp-17-4887-2017
- 681 Marke, T., Crewell, S., Schemann, V., Schween, J. H., & Tuononen, M. (2018).
 682 Long-Term Observations and High-Resolution Modeling of Midlatitude
 683 Nocturnal Boundary Layer Processes Connected to Low-Level Jets. *Jour-
 684 nal of Applied Meteorology and Climatology*, *57*(5), 1155-1170. doi:
 685 10.1175/JAMC-D-17-0341.1
- 686 Moeng, C.-H., Cotton, W. R., Bretherton, C., Chlond, A., Khairoutdinov, M.,
 687 Krueger, S., ... Sykes, R. I. (1996). Simulation of a stratocumulus-
 688 topped planetary boundary layer: Intercomparison among different numerical
 689 codes. *Bulletin of the American Meteorological Society*, *77*(2), 261-278. doi:
 690 10.1175/1520-0477(1996)077<0261:SOASTP>2.0.CO;2
- 691 Moeng, C. H., Dudhia, J., Klemp, J., & Sullivan, P. (2007, June). Examining Two-
 692 Way Grid Nesting for Large Eddy Simulation of the PBL Using the WRF
 693 Model. *Mon Weather Rev*, *135*(6), 2295–2311.
- 694 Neggers, R. A. J., Chylik, J., Egerer, U., Griesche, H., Schemann, V., Seifert, P.,
 695 ... Macke, A. (2019). Local and remote controls on arctic mixed-layer evolu-
 696 tion. *Journal of Advances in Modeling Earth Systems*, *11*(7), 2214-2237. doi:
 697 10.1029/2019MS001671
- 698 Neggers, R. A. J., Siebesma, A. P., & Heus, T. (2012). Continuous single-column
 699 model evaluation at a permanent meteorological supersite. *Bulletin of the*

- 700 *American Meteorological Society*, 93(9), 1389-1400. Retrieved from <https://doi.org/10.1175/BAMS-D-11-00162.1> doi: 10.1175/BAMS-D-11-00162.1
- 701
- 702 Reilly, S., Gesso, S. D., & Neggers, R. (2020). Configuring les based on dropsonde
703 data in sparsely sampled areas in the subtropical atlantic. *Journal of Applied
704 Meteorology and Climatology*, 59(2), 297-315. doi: 10.1175/JAMC-D-19-0013
705 .1
- 706 Satoh, M., Stevens, B., Judt, F., Khairoutdinov, M., Lin, S.-J., Putman, W. M., &
707 Düben, P. (2019, May). Global Cloud-Resolving Models. *Curr Clim Change
708 Rep*, 5(3), 172-184.
- 709 Schalkwijk, J., Jonker, H. J. J., Siebesma, A. P., & Bosveld, F. C. (2015). A year-
710 long large-eddy simulation of the weather over cabauw: An overview. *Monthly
711 Weather Review*, 143(3), 828-844. doi: 10.1175/MWR-D-14-00293.1
- 712 Schemann, V., & Ebell, K. (2020). Simulation of mixed-phase clouds with
713 the ICON large-eddy model in the complex Arctic environment around
714 Ny-Ålesund. *Atmospheric Chemistry and Physics*, 20(1), 475-485. doi:
715 10.5194/acp-20-475-2020
- 716 Schneider, T., Lan, S., Stuart, A., & Teixeira, J. (2017). Earth System Modeling
717 2.0: A Blueprint for Models That Learn From Observations and Targeted
718 High-Resolution Simulations. *Geophys. Res. Lett.*, 44(24), 12,396-12,417.
- 719 Seifert, A., & Beheng, K. D. (2006, Feb 01). A two-moment cloud microphysics pa-
720 rameterization for mixed-phase clouds. part 1: Model description. *Meteorology
721 and Atmospheric Physics*, 92(1), 45-66. doi: 10.1007/s00703-005-0112-4
- 722 Stevens, B., Acquistapace, C., Hansen, A., Klinger, C., Klocke, D., Schubotz, W.,
723 ... Biercamp, J. (2020). Large-eddy and Storm Resolving Models for Climate
724 Prediction – The Added Value for Clouds and Precipitation. *Journal of the
725 Meteorological Society of Japan. Ser. II*, 1-115.
- 726 Stevens, B., Satoh, M., Auger, L., Biercamp, J., Bretherton, C. S., Chen, X., ...
727 Zhou, L. (2019, September). DYAMOND: the DYnamics of the Atmospheric
728 general circulation Modeled On Non-hydrostatic Domains. *Prog. in Earth and
729 Planet. Sci.*, 6(1), 1-17.
- 730 Stevens, B., Sherwood, S. C., Bony, S., & Webb, M. J. (2016, November). Prospects
731 for narrowing bounds on Earth’s equilibrium climate sensitivity. *Earth’s Fu-
732 ture*, 4(11), 512-522.
- 733 Talbot, C., Bou-Zeid, E., & Smith, J. (2012, October). Nested Mesoscale Large-
734 Eddy Simulations with WRF: Performance in Real Test Cases. *J. Hydrome-
735 teor*, 13(5), 1421-1441.
- 736 van Laar, T. W., Schemann, V., & Neggers, R. A. J. (2019). Investigating the diur-
737 nal evolution of the cloud size distribution of continental cumulus convection
738 using multiday les. *Journal of the Atmospheric Sciences*, 76(3), 729-747. doi:
739 10.1175/JAS-D-18-0084.1
- 740 Warner, T. T., Peterson, R. A., & Treadon, R. E. (1997). A tutorial on lateral
741 boundary conditions as a basic and potentially serious limitation to regional
742 numerical weather prediction. *Bulletin of the American Meteorological Society*,
743 78(11), 2599-2618. doi: 10.1175/1520-0477(1997)078<2599:ATOLBC>2.0.CO;2